GEORG-AUGUST-UNIVERSITÄT
GÖTTINGEN

Bachelor's Thesis

Teilchensimulationen von Polymermischungen in begrenzten Geometrien mit zeitabhängigen Randbedinungen

Particle simulations of polymer mixtures in confined geometries with time dependent boundary conditions

prepared by

Justus Multhaup

from Holzminden

at the Institut für Theoretische Physik

Thesis period: 1st April 2023 until 30th June 2023

First Rreferee: Prof. Dr. Marcus Müller

Second referee: Prof. Dr. Stefan Klumpp

Contents

Nomenclature

Acronyms

GPU	Graphics processing unit	13
MC	Monte-Carlo	1
MD	Molecular Dynamics	1
NESS	non-equilibrium steady state	15
SA	Simulated Annealing	29
SCFT	Self-Consistent Field Theory	13
SCMF	Single-Chain-in-Mean-Field	2
SMC	Smart Monte-Carlo	13
SOMA	SOft coarse-grained Monte-Carlo Acceleration	2
SSL	Strong-segregation limit	8
WSL	Weak-segregation limit	8

1. Introduction

- Still the old version from Einfuehrung ins Wissenschaftliche Arbeiten

Polymers are highly versatile macromolecules composed of repeating units called monomers. Their importance for life on earth cannot be overstated, biological polymers are involved in countless chemical reactions in the human body and form the backbone of proteins and DNA. Synthetic polymers are applied almost everywhere in modern society, ranging from simple packaging materials to highly sophisticated materials used in aerospace engineering. This is owed to their vast range of unique physical properties, such as high elasticity, flexibility and durability. When creating novel materials with very precise features, understanding how polymers interact with one another and form structure via phase separation in multicomponent systems is essential.
One important class of polymers is the so-called homopolymer, which is made of a single type of monomer unit, for example, polyethylene. Copolymers, in contrast, consist of two or more different types of monomer units. Copolymers that are concatenations of homopolymers of different types and lengths are called block-copolymers. One of the most interesting and extensively studied properties of copolymers is their ability to self-assemble into microphases [13]. An important tool in understanding the mechanisms behind this microphase separation, and many other interesting properties, is the use of computer simulations. These include particle-based Molecular Dynamics (MD) and Monte-Carlo (MC) methods as well as continuum-model-based and hybrid methods [21]. Particle-based simulations accurately model small-scale phenomena. However, despite rapid advancements in computer technology and high parallelizability, they are too computationally expensive to simulate long time scales since they involve the explicit calculation of the strong, bonded interactions between particles. This also poses limitations on the system size; macro scale phenomena are hard to capture. Continuum models, on the other hand, are less computationally expensive, but at the cost of a lower accuracy on the microscale. On the mesoscale, good agreement between the two types

of models was observed, e.g. in the orientation of cylindrical mesophases upon solvent evaporation [7]. To evaluate the accuracy of continuum models on small-length scales, it is necessary to compare them to established particle-based models. One approach to this is to consider a simulation box in a particle-based simulation as a small section from a large continuum-model-based simulation. The dynamics are then driven by extracting the time evolution of the density fields at the boundaries from the continuum simulation and applying them in the particle-based simulation, e.g. employing non-periodic boundary conditions. However, dictating the boundary densities in particle-based simulations is not a trivial task. One option is the use of external fields or the umbrella sampling method [28], although this has the large drawback that the number of particles in the simulation box remains constant, while in the continuum simulation particles can enter and leave the section at any time. An alternative is to employ conversion zones at the boundaries, in which molecules are converted to different types, mimicking particle exchange with the surrounding as shown in Figure 1.1. If the densities are defined on a discretized grid, this leads to an optimization problem in which the ideal configuration of molecule types needs to be found, such that the mean squared deviation from the target density is minimized.

In this study, as a first step towards boundary-driven particle simulations, the dynamics of noninteracting homopolymers are investigated. Specifically, a system is pushed away from equilibrium by introducing conversion zones at the boundary regions of the simulation box. This results in a diffusive current and allows the calculation of the collective diffusion coefficient of the system. To this end, the SOft coarse-grained Monte-Carlo Acceleration (SOMA) [25] software package based on the Single-Chain-in-Mean-Field (SCMF) algorithm [5] is employed.

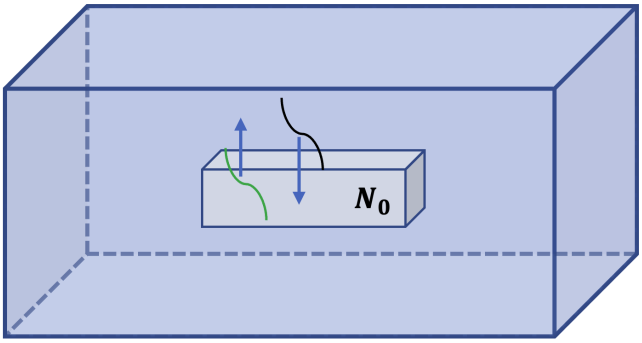

Figure 1.1.: Sketch of the setting explained in the text. Polymers of different types may be exchanged with the surrounding, but the number of molecules N_0 inside the section of the particle simulation remains constant.

2. Theory

2.1. Single-chain properties

Since the collective dynamics of polymer mixtures can often be directly related to the single-chain properties, some selected aspects are briefly discussed here. The simplest model to describe a polymer chain is the ideal chain, for which any non-bonded interaction between monomers is neglected.

2.1.1. The freely jointed chain

The freely jointed chain model is an ideal model in which the chain is composed of N segments of length a, whose orientation vectors $\mathbf{r}_i$ ($a = |\mathbf{r}_i|$) can face in any direction and are completely independent from each other. The chain configuration may be characterised by the *end-to-end-vector* $\mathbf{R}$:

$$\mathbf{R} = \sum_{i=1}^{N} \mathbf{r}_i \,. \tag{2.1}$$

Due to the completely random orientation, $\mathbf{R}$ has zero mean. A useful property to quantify the spatial extension of the chain is the mean square of $\mathbf{R}$, which calculates to:

$$R_e^2 \equiv \langle \mathbf{R}^2 \rangle = Na^2 \,. \tag{2.2}$$

For large N, $\mathbf{R}$ has a Gaussian distribution [14]:

$$P(N, \mathbf{R}) = \left(\frac{3}{2\pi R_e^2} \right)^{3/2} \exp\left[-\frac{3\mathbf{R}^2}{2R_e^2} \right] , \tag{2.3}$$

the freely jointed chain therefore converges towards the Gaussian chain.

2.1.2. Rouse model

The Rouse model [24] is used to describe the dynamics of a Gaussian chain moving through a solvent. The stiff bonds are replaced by springs of root-mean-square size b, through which a monomer interacts with its neighbours. The monomers experience a friction force with friction coefficient ζ, and the total friction coefficient of the center of mass is:

$$\zeta_{\mathrm{R}} = N\zeta\,. \tag{2.4}$$

Within the Rouse model, the diffusion coefficient of the chain is computed as:

$$D_{\mathrm{R}} = \frac{k_B T}{\zeta_{\mathrm{R}}} = \frac{k_B T}{N\zeta}\,. \tag{2.5}$$

For an n-dimensional diffusion of a Brownian particle, the single chain diffusion constant is related to the mean squared displacement of the chain center of mass $g_3(t)$ by the Einstein relation [9]:

$$\begin{aligned} D &= \frac{g_3(t)}{2nt}\,, \\ g_3(t) &= \langle (\mathbf{r}_{cm}(t) - \mathbf{r}_{cm}(t_0))^2 \rangle\,, \end{aligned} \tag{2.6}$$

where $\mathbf{r}_{cm}(t)$ is the center of mass position at time t and t_0 is the time at which the measurement is started. The time in which a polymer diffuses a distance of the order of its size is called relaxation time τ_{R}:

$$\tau_{\mathrm{R}} \approx \frac{R_e^2}{D_{\mathrm{R}}} = \frac{\zeta}{k_B T} N R_e^2\,. \tag{2.7}$$

On time scales larger than τ_{R}, the chain movement is only due to diffusion, while viscoelastic effects are observed at shorter time scales.

2.2. Polymeric mixtures

Polymer mixtures consist of two or more chemically different polymer types. The mechanical and thermodynamic properties can vary greatly with several factors such as composition, molecular weight and interactions between the polymers. This makes them desirable for manufacturing materials with tailored properties.
If the composition is uniform everywhere, the mixture is called homogeneous. In a heterogeneous mixture, in contrast, the composition is non-uniform, leading to visible boundaries which may have very different properties. This phenomenon is also called macro-phase separation. From an entropic viewpoint, mixing is always favored. However, energetic interactions between polymers may either favor or suppress mixing. Whether a mixture is homogeneous or heterogeneous, thus, depends on the balance between entropy and energy [14, S. 137].

2.2.1. Flory-Huggins Theory

Whether mixing or phase separation will be favored can be predicted by determining the free-energy change associated with mixing the components. This free energy-change can be computed within the lattice model developed by Flory and Huggins [11]. Within the Flory-Huggins framework, no volume change is assumed upon mixing. With this assumption, it is convenient to represent the system on a lattice. A lattice site corresponds to the smallest molecular unit and every macromolecule takes up one or multiple lattice sites. Consider a binary mixture with n_A polymers of species A and chain length N_A and n_B polymers of species B and chain length N_B. Let the total number of polymers be $n = n_\mathrm{A} + n_\mathrm{B}$. The free energy of mixing per monomer ΔF_{mix} is then given by the Flory-Huggins equation of polymer solutions [14, S. 143]:

$$\frac{\Delta F_{mix}}{k_B T} = \frac{\phi}{N_\mathrm{A}} \ln \phi + \frac{1-\phi}{N_\mathrm{B}} \ln(1-\phi) + \chi\phi(1-\phi)\,. \tag{2.8}$$

Here, $\phi = n_\mathrm{A} N_\mathrm{A}/(n_\mathrm{A} N_\mathrm{A} + n_\mathrm{B} N_\mathrm{B})$ is the monomer fraction of species A, k_B is the Boltzmann constant, T is the system temperature and χ is the Flory interaction parameter which characterizes the interaction between different polymer species and can be obtained from experiments. A positive value of χ opposes mixing while a negative value promotes it; knowing the value of χ, therefore, allows us to qualitatively

predict the phase separation behavior. For $\chi = 0$, (2.8) reduces to regular solution theory for an ideal gas of polymers with concentrations ϕ/N_A and $(1-\phi)/N_B$. Note that so far, no space dependency of ϕ has been assumed. In the following discussion, a symmetric mixture with $N_\mathrm{A} = N_\mathrm{B} = N$ is assumed. To fully capture the complexity of the system, the Flory-Huggins model has to be extended to include spatial variations of ϕ, which gives rise to the de Gennes-Flory-Huggins free-energy functional [6, 22]:

$$\frac{F[\phi]R_e^3}{k_B T\sqrt{\bar{N}}} = \int \mathrm{d}^3\mathbf{r} \left\{ \phi \ln \phi + (1-\phi)\ln(1-\phi) + \chi N \phi(1-\phi) + k(\phi)[\nabla\phi]^2 \right\} . \quad (2.9)$$

Here, $\bar{N} = \left(nR_e^3/V\right)^2$ is the invariant degree of polymerization of the system with volume V. It is a measure of the number of neighboring chains a chain interacts with. The term proportional to $[\nabla\phi]^2$ is added to the free-energy density to ensure that unphysical, sharp changes in the local densities are penalized. The precise form of $k(\phi)$ depends on the strength of the parameter χ. For small $\chi N \lesssim 5$, one considers the Weak-segregation limit (WSL). For large $\chi N \gtrsim 10$ [26], the Strong-segregation limit (SSL) holds. In these two limits, the prefactor k takes the following form [22]:

$$k_\mathrm{WSL} = \frac{R_e^2}{36\phi(1-\phi)} ; \qquad k_\mathrm{SSL} = \frac{R_e^2}{24\phi(1-\phi)} . \quad (2.10)$$

2.3. Collective diffusion

Consider again a binary mixture of polymers with $N_\mathrm{A} = N_\mathrm{B} = N$. Since the number of polymers in the system is constant, the continuity equation holds:

$$\frac{\partial\phi}{\partial t} + \nabla \cdot \mathbf{J}_\mathrm{A} = 0 . \quad (2.11)$$

Here, $\mathbf{J}_\mathrm{A}$ is the local current of polymer species A. Near equilibrium, one postulates a linear relation between $\mathbf{J}_\mathrm{A}$ and the local chemical potential μ_A [6]. In the most general case, this relation is non-local in space and time. Assuming translational invariance in space and time, it reads [10]:

$$\mathbf{J}_\mathrm{A}(\mathbf{r},t) = -\int_{t'=-\infty}^{t} \mathrm{d}t' \int_V \mathrm{d}\mathbf{r}' \, \frac{\Lambda_\mathrm{A}(\mathbf{r}-\mathbf{r}', t-t')}{k_B T} \nabla' \mu_\mathrm{A}(\mathbf{r}', t') \,. \tag{2.12}$$

The Onsager coefficient $\Lambda_\mathrm{A}(\mathbf{r}-\mathbf{r}', t-t')$ relates the gradient of the chemical potential at position $\mathbf{r}'$ to a density flux at position $\mathbf{r}$ and also accounts for memory effects. The non-localities in (2.12) translate into a dependency of Λ on the wave vector $\mathbf{q}$ and the frequency ω in Fourier space. In the time-independent steady state, this gives:

$$\mathbf{J}_{\mathrm{A},q} = -iq \frac{\Lambda_{\mathrm{A},q}}{k_B T} \mu_{\mathrm{A},q} \,, \tag{2.13}$$

where $q = |\mathbf{q}|$. In the following, it is assumed that $\mu[\phi(x)] \propto x$, so $\mu_q \propto 1/q$ and $\nabla\mu = \mathrm{const}$. For a spatially independent current, this implies that Λ must also be independent of q , so in the spatial picture:

$$\mathbf{J}_\mathrm{A} = -\frac{\Lambda_\mathrm{A}}{k_B T} \nabla \mu_\mathrm{A} \,. \tag{2.14}$$

This approximation holds for small q and therefore prohibits the probing of the q-dependence of Λ , but it leads to a simple form of the Onsager coefficient that will be derived in the following.

Following the discussion in the appendix of [6], consider a mixture of polymer chains with densities ϕ_A and ϕ_B . Incompressibility, e.g. $\phi_\mathrm{A} + \phi_\mathrm{B} = 1$, is enforced by introducing an additional repulsive potential U to the chemical potential, so from (2.14) one obtains:

$$\mathbf{J}_\mathrm{A} = -\Lambda_\mathrm{A} \nabla[(\mu_\mathrm{A} + U)/k_B T] \,, \tag{2.15a}$$

$$\mathbf{J_B} = -\Lambda_\mathrm{B} \nabla[(\mu_\mathrm{B} + U)/k_B T] \,. \tag{2.15b}$$

Due to the incompressibility, the total current $\mathbf{J} = \mathbf{J}_\mathrm{A} + \mathbf{J}_\mathrm{B}$ must have zero divergence, which in one dimension means $\mathbf{J} \equiv J\mathbf{e_x} = \mathrm{const}$. From the Galilei invariance of the system, we can simply choose $J = 0$. From this condition, U can

be calculated explicitly:

$$U = (\Lambda_\mathrm{A}\mu_\mathrm{A} + \Lambda_\mathrm{B}\mu_\mathrm{B})/(\Lambda_\mathrm{A} + \Lambda_\mathrm{B})\,. \tag{2.16}$$

Since one of the currents is redundant, write $J \equiv J_A$. From (2.15), obtain:

$$J = -\Lambda\nabla(\mu_\mathrm{A} - \mu_\mathrm{B}) \equiv -\Lambda\nabla\mu\,, \tag{2.17}$$

where $\Lambda = \Lambda_\mathrm{A}\Lambda_\mathrm{B}/(\Lambda_\mathrm{A} + \Lambda_\mathrm{B})$ and μ is the exchange chemical potential. In the limit of no interactions, the mixture can be considered as an ideal gas, so $\Lambda_i = D_i/\phi_i$ for $i = \mathrm{A}, \mathrm{B}$. For $D_\mathrm{A} = D_\mathrm{B} \equiv D$, this yields:

$$\Lambda = D\phi(\mathbf{r})(1 - \phi(\mathbf{r}))\,. \tag{2.18}$$

This approximation is frequently used in the literature for the sake of computational efficiency [4, 6, 12]. It corresponds to a local coupling in which monomers move like the center of mass, therefore it does not account for the connectivity of the monomers along the backbone of the chain.

2.4. Single chain in mean field simulations

- Briefly explain SCMF basics, either here or in introduction
- **paraphrase!!**

Although the soft, coarse grained model used in this thesis provides a high flexibility in molecular architectures, the following discussion is restricted to symmetric AB-diblock copolymers in a volume V at temperature T for simplicity. The partition function in the canonical ensemble takes the form:

$$\mathcal{Z} \propto \frac{1}{n!}\int\prod_{i=1}^{n}\mathcal{D}[\mathbf{r}_i(s)]\mathcal{P}_0[\mathbf{r}_i(s)]\exp\left(\frac{-\mathcal{H}_\mathrm{nb}[\hat{\phi}_\mathrm{A}, \hat{\phi}_\mathrm{B}]}{k_B T}\right), \tag{2.19}$$

where $\mathbf{r}_i(s)$ with $i = 1, \ldots, n$ is the position of segment s that belongs to molecule i. The factor $\int \mathcal{D}[\mathbf{r}_i(s)] \equiv \int \prod_s d^3\mathbf{r}_i(s)$ accounts for the different configurations that molecule i can take $P_0[\mathbf{r}_i(s)] \propto \exp\left(-\mathcal{H}_\mathrm{b}[\mathbf{r}_i(s)]/k_BT\right)$ is the probability distribution of configurations in the abscence of non-bonded interactions. For Gaussian polymers, the bonded interactions $\mathcal{H}_\mathrm{b}[\mathbf{r}_i(s)]$ are modeled by the following discretized Hamiltonian:

$$\frac{\mathcal{H}_\mathrm{b}[\mathbf{r}_i(s)]}{k_BT} = \sum_{s=1}^{N-1} \frac{3(N-1)}{2R_e^2}[\mathbf{r}_i(s) - \mathbf{r}_i(s+1)]\,. \tag{2.20}$$

The non-bonded interactions depend on the local, normalised monomer densities, $\hat{\phi}_\mathrm{A}$ and $\hat{\phi}_\mathrm{B}$, and are modeled by the following excess interaction free energy functional:

$$\frac{\mathcal{H}_\mathrm{nb}[\hat{\phi}_\mathrm{A}, \hat{\phi}_\mathrm{B}]}{k_BT} = \frac{\rho_0}{N}\int_V d^3\mathbf{r}\left(\frac{\kappa N}{2}[\hat{\phi}_\mathrm{A} + \hat{\phi}_\mathrm{B} - 1]^2 - \frac{\chi N}{4}[\hat{\phi}_\mathrm{A} - \hat{\phi}_\mathrm{B}]^2\right)\,, \tag{2.21}$$

where $\rho_0 = \frac{nN}{V}$ is the average monomer density, κ describes the the compressibility of the system and χ is the Flory-Huggins parameter. The first term in the integrand penalises excluded volume and thus determines the compressibility, the second term describes the repulsion of monomers of different types. The densities $\hat{\phi}_{\alpha,m}$ ($\alpha = \mathrm{A}, B$) are defined on a cubic grid with spacing ΔL, the total number of cells is $N_{cells} = V/(\Delta L)^3$. With $\mathbf{c}_m$ being the center of the mth cell, one can write:

$$\hat{\phi}_{\alpha,m} = \sum_{i=1}^{n}\sum_{s=1}^{N}\Pi(\mathbf{r}_i(s), \mathbf{c}_m)\gamma_\alpha(s)\,, \tag{2.22}$$

where $\gamma_\alpha(s) = 1$ if the sth segment is of type α and $\gamma_\alpha(s) = 0$ otherwise. $\Pi(\mathbf{r}_i(s), \mathbf{c}_m)$ is the characteristic function of the grid cell. This way, (2.21) may be discretized in the following way:

$$\frac{\mathcal{H}_\mathrm{nb}[\hat{\phi}_\mathrm{A}, \hat{\phi}_\mathrm{B}]}{k_BT} = \frac{\rho_0\Delta L^3}{N}\sum_{m=1}^{N_{cells}}\left(\frac{\kappa N}{2}[\hat{\phi}_{\mathrm{A},m} + \hat{\phi}_{\mathrm{B},m} - 1]^2 - \frac{\chi N}{4}[\hat{\phi}_{\mathrm{A},m} - \hat{\phi}_{\mathrm{B},m}]^2\right)\,. \tag{2.23}$$

2.5. Smart Monte Carlo move

- to be extended

The friction from the Rouse model can be incorporated into MC simulations by using a Smart Monte Carlo (SMC) scheme [20]. The particle positions are proposed according to:

$$\mathbf{r}_i'(s) = \mathbf{r}_i(s) + \frac{\Delta t}{\zeta}\mathbf{F}_i(\mathbf{r}) + \Delta\mathbf{r}\,, \tag{2.24}$$

where $\Delta\mathbf{r}$ is from the usual MC algorithm and $\mathbf{F}_i(s)$ is the bonded force acting on the segment. Δt is the time step of the simulation and ζ controls the segmental friction. The value of Δt , that maximizes the MC acceptance rate, was found to be $\Delta t = 0.17(\zeta R_e^2/Nk_BT)$ [18].

3. Simulation technique

- Still the old version from Einfuehrung ins Wissenschaftliche Arbeiten

To simulate the collective dynamics, a coarse-grained model of the polymers is employed. Within this model, several monomeric repeat units are grouped into an effective interaction center, called *bead*, which allows for an efficient numerical implementation. Nevertheless, in this study, the terms "bead" and "monomer" will be used interchangeably. A great variety of universal properties of polymeric materials on mesoscopic length scales is accurately captured by coarse-grained models [2].
The software package that is used for the numerical calculations, SOMA [25], uses a combination of a coarse-grained model and the SCMF algorithm [5]. Unlike the widely used Self-Consistent Field Theory (SCFT), the SCMF method includes fluctuation effects which are required to accurately describe certain systems and effects, e.g. dilute polymer solutions, the vicinity of phase transitions, or polymeric microemulsions [3, 8, 16]. Instead of calculating the interaction of a chain with all its surrounding explicitly, the chains are subjected to fluctuating external fields which are frequently recalculated from the density distribution. The densities are defined on a cubic grid. The time evolution of the system is then performed by MC simulation and the external fields remain constant during one MC sweep, this is called *quasi-instantaneous field approximation*. The enormous benefit of this is that the chains are decoupled, making it possible to implement it effectively on parallel machines and leverage accelerators like Nivida Graphics processing units (GPUs) [25]. Additionally, Smart Monte-Carlo (SMC) scheme is employed that uses the strong bonded forces to propose a trial displacement resembling Brownian motion and produces Rouse-like dynamics [19, 23].
While a full description of the SCMF equations can be found in [5], and will be omitted here, it is important to note that the interactions are fully described by three coarse-grained parameters: the average mean squared end-to-end distance R_e^2 of a chain in the absence of non-bonded interactions, the inverse thermal compressibility $\kappa_o N$ and the incompatibility between different bead types $\chi_o N$. The term "soft" in

SOMA relates to the soft nature of the non-bonded interactions, which arises from the systematic coarse-graining and allows for an overlap of beads [17].

4. Collective diffusion of symmetric homopolymers

4.1. Reference system

In this section, the collective diffusion properties of noninteracting homopolymers with $N_\mathrm{A} = N_\mathrm{B} = N$ and $\chi = 0$ are investigated. As a reference system, a simulation box with $n = 10000$ polymers and dimensions $L_x \times L_y \times L_z = 9.75 \times 3 \times 3\, R_e^3$ is used, so the invariant degree of polymerization is $\sqrt{\bar{N}} \approx 114$. The spatial discretization is $\Delta L = 0.125\, R_e$. Periodic boundary conditions are applied in the lateral y and z directions, whereas impenetrable walls are applied in the x direction. Initially, the polymers are distributed homogeneously in the system. To stimulate a flux in a non-equilibrium steady state (NESS), conversion zones of width $d = 0.25\, R_e$ are introduced close to the walls. In each time step, if the center-of-mass coordinate $\mathbf{r}_{cm}$ of a polymer of type A lies in the left conversion zone, it is converted to type B with probability $p(A \to B) = r$. Analogously, conversion from B to A takes place in the right conversion zone with the same probability r. The current $\mathbf{J}$ is measured by tracking the number of polymer conversions. The simulation setup is depicted in Figure 4.1.

The computation of the transport properties is complicated by boundary effects, such as a steep density drop close to the hard walls, which is of entropic origin. Furthermore, chains whose center of mass lies in the conversion zone may extend far beyond that zone. The range of these effects is approximated as R_e and measurements are only taken in the region where the effects are negligible.

4.2. Collective diffusion coefficient

Due to the periodic boundary conditions and the spatial homogeneity in the lateral directions, the system can effectively be described in one dimension. The density

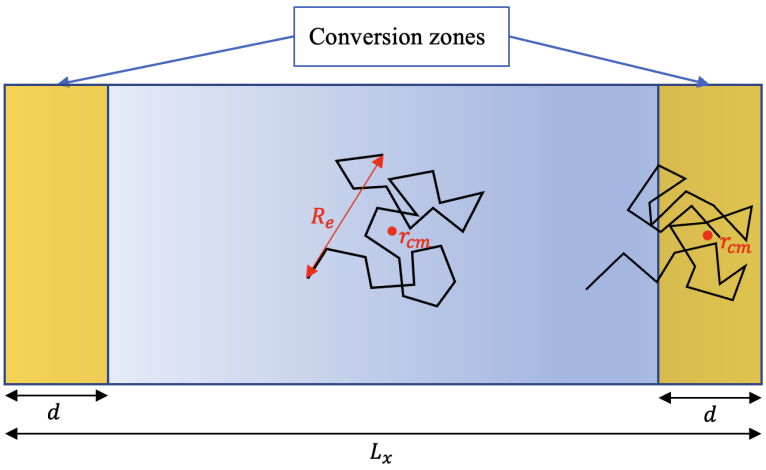

Figure 4.1.: Simulation setup. For clarity, the conversion zones are not to scale and no distinction between polymer types is made.

profile for $r = 1.0$ is shown in Figure 4.2.

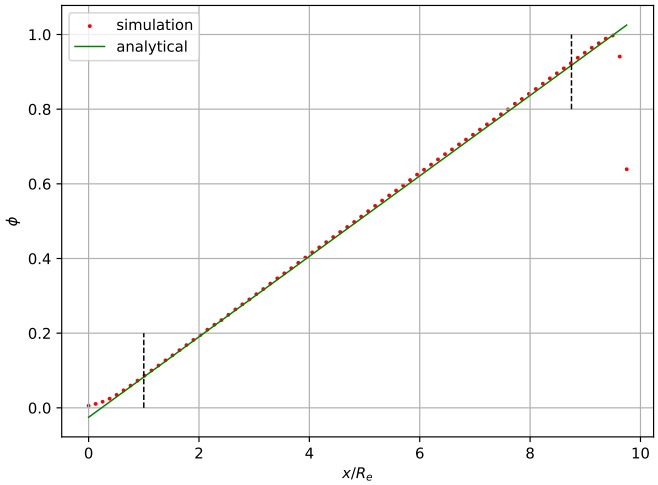

Figure 4.2.: Steady-state density profile for $r = 1.0$ averaged over y and z. The analytical curve corresponds to (4.4). The black lines mark the region that is estimated to be affected by boundary effects.

Outside of the range of the boundary effects, the density profile is very well represented by a linear function. The chemical potential is obtained by taking the functional derivative $\frac{\delta F}{\delta \phi}$ of (2.9). Since $\chi = 0$, no phase separation occurs and the local density differences are entirely due to the dynamics. Assuming the WSL, the chemical potential becomes:

$$\frac{\mu R_e^3}{\sqrt{\bar{N}} k_B T} = \ln\phi - \ln(1-\phi) - \frac{R_e^2}{18\phi(1-\phi)}\phi'' + \left[\frac{R_e^2(1-2\phi)}{36\phi^2(1-\phi)^2}\right]\phi'^2 , \tag{4.1}$$

where the dashes denote derivatives with respect to x. The resulting chemical potential profile is shown in Figure 4.3a.

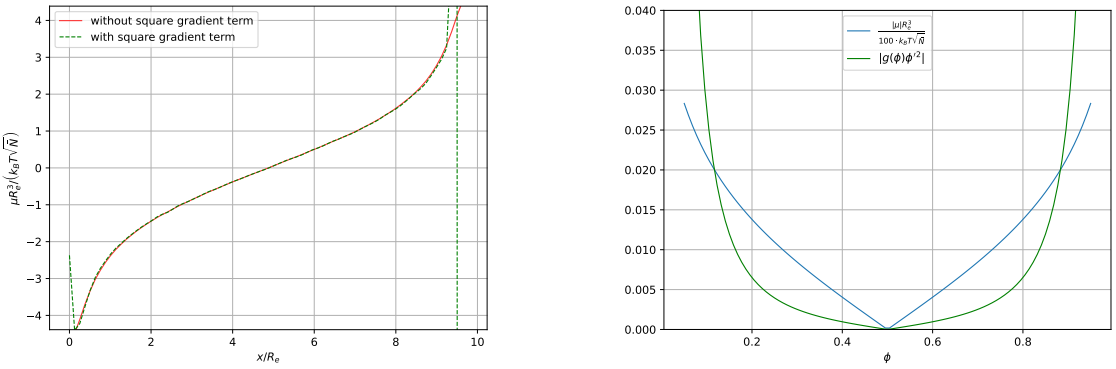

(a) (b)

Figure 4.3.: (a) Steady-state chemical potential profile obtained from (4.1) for $r = 1.0$, averaged over y and z. (b) $g(\phi)\phi'^2 \equiv R_e^2(1-2\phi)\phi'^2/[36\phi^2(1-\phi)^2]$ and absolute value of chemical potential $|\mu|R_e^3/(100 \cdot k_B T\sqrt{\bar{N}})$. In the discussed case, $\phi' \approx 0.1$.

Evidently, the contribution of the terms involving spatial derivatives of the density to the total chemical potential is negligible, except in a very small region close to the walls. The linearity of the density profile already implies $\phi'' = 0$ and Figure 4.3 shows that the term proportional to ϕ'^2 accounts for less than one percent of the total chemical potential for $0.12 \lesssim \phi \lesssim 0.88$, which roughly corresponds to the region in Figure 4.2 that is assumed to be unaffected by boundary effects. In the subsequent discussion, the terms in (4.1) containing spatial derivatives of ϕ will be neglected. This approximation improves further as the simulation box becomes infinitely long and $\phi' \to 0$. However, for more complex density profiles, the contribution is of course not negligible.

With (2.14) and (4.1), neglecting the terms arising from the square gradient, the current becomes:

$$J = -D\sqrt{\bar{N}}R_e^{-3}\phi' \,, \tag{4.2}$$

Together with (2.11), this gives the standard diffusion equation:

$$\frac{\partial\phi(\mathbf{r},t)}{\partial t} - D\phi'' = 0 \,. \tag{4.3}$$

where D is obtained from (2.7). In the steady state, this simply yields $\phi'' = 0$, so a linear density profile is obtained, as expected. From (4.2) and the condition that $\phi(L_x/2) = 1/2$, which follows from the symmetry of the conversion rates, the density profile becomes:

$$\phi(x) = \frac{JR_e^3}{D\sqrt{\bar{N}}}\left(\frac{L_x}{2} - x\right) + \frac{1}{2} \,, \tag{4.4}$$

To verify (2.18), the Onsager coefficient may also be obtained directly from the simulation results using (2.14). Again assuming local coupling and making use of (4.1), while neglecting the terms arising from the square gradient, one obtains:

$$\Lambda = -\frac{JR_e^3}{\sqrt{\bar{N}}\phi'}\phi(1-\phi). \tag{4.5}$$

The resulting Onsager coefficient is plotted in Figure 4.4.

The Onsager coefficients obtained from (2.18) and (4.5) are in excellent agreement, which hints that the theoretical derivations are consistent with the simulation results. Specifically, the assumptions of incompressibility and local coupling of the current to the chemical potential are justified and the linear density profile observed in Figure 4.2 is explained.

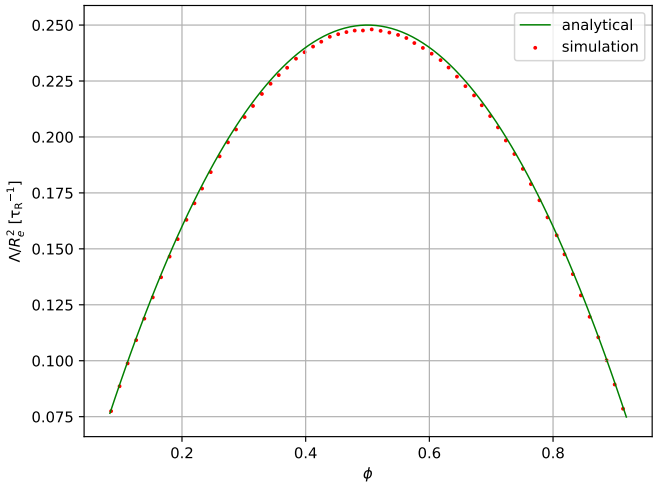

Figure 4.4.: Onsager coefficient Λ as a function of ϕ. The analytical curve is obtained from (2.18) and (4.4), the numerical curve from (4.5) and the density profile in 4.2, where ϕ' is obtained from a linear fit. Only data points measured at a distance greater than R_e from the walls are used. The diffusion constant D and the current J are both obtained from the simulation.

5. External-field-driven flow

One of the simplest ways to implement time-dependent boundary conditions in SOMA is to apply time-dependent external fields that are only nonzero close to the boundaries and have the form:

$$E_i(\mathbf{r}, t) = f_i(\mathbf{r}, t)\phi_i(\mathbf{r}, t)\,, \tag{5.1}$$

where $i = \mathrm{A}, \mathrm{B}$ denotes the monomer types. In this section, layers of lamellar diblock-copolymers are moved at constant speed v perpendicular to their orientation using spatially periodic external fields close to the boundaries. In a system that moves along with the external field, each monomer experiences a friction force ζv in the opposite direction, where ζ is obtained from (2.5). The degree of deformation depends on the Péclet number $P_e \equiv vR_e/D$. For large values $P_e \approx 1$, the chains cannot keep up with the external field movement and the lamellae break. For small $P_e \approx 0$, they have enough time to fully relax to the undeformed shape. In this section, an intermediate regime is investigated to obtain the bending modulus K.

5.1. Reference system

A system of $n = 750$ symmetric diblock-copolymers with $N_A = N_B = N/2 = 16$ and $\chi N = 20$ is used. The box dimensions are $L_x \times L_y \times L_z = 2.5 \times 2.82 \times 1\, R_e^3$, which corresponds to $\sqrt{N} = 106$. The spatial discretizations are $\Delta x = 1/16\, R_e$, $\Delta y = 47/800\, R_e$ and $\Delta z = 1\, R_e$. To generate the initial lamellar structure, external fields are applied, as shown in Figure 5.1. The interlayer spacing of $d = 1.41\, R_e$ was found to be stable over the duration of the simulations, but it does not correspond to the equilibrium spacing.

Subsequently, the external fields are switched off everywhere except at a distance less than $b = 0.5\, R_e$ from the boundaries in the x-direction, so the length of the part

of the lamellae that is not supported by the external fields is $L = 1.5\,R_e$. Every Δt MCS, the fields are moved by a distance of Δy in the y-direction, so the velocity is $v = 47R_e/(800\Delta t)$. The external fields balance the friction forces at the boundaries and therefore act as bearings for the lamellae. The diffusion constant D is obtained from (2.7), where $g_3(t)$ is measured in a system without external fields and $\chi N = 0$.

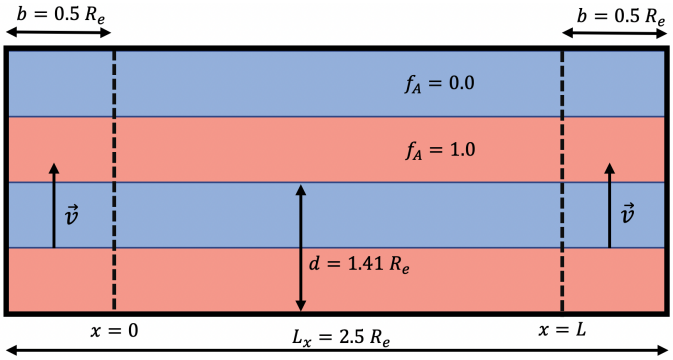

Figure 5.1.: Sketch of the external field $f_{\mathrm{A}}(\mathbf{r}, 0)$. Red domains correspond to $f_{\mathrm{A}} = 1.0$, blue domains to $f_{\mathrm{A}} = 0.0$. $f_{\mathrm{B}}(\mathbf{r}, 0)$ is exactly complementary. Within the region bounded by the dotted lines, the external fields are switched off after the initial lamella structure has been generated.

5.2. Bending modulus

For small deformations, in the SSL, the free energy of a bent lamella is [29]:

$$F = \int d\mathbf{r} \left\{ f_0 + \frac{1}{2} K \left(\partial_x^2 u \right)^2 \right\} , \tag{5.2}$$

$$\approx dL_z \int dx \left\{ f_0 + \frac{1}{2} K \left(\partial_x^2 u \right)^2 \right\}$$

$$\equiv dL_z \int dx f(u, u'') . \tag{5.3}$$

where f_0 is the free energy per unit volume of the unbent lamella, K is the bending modulus and $u \equiv u(x)$ is the deformation profile of the A-B-interface. For the integration over y and z, the change of volume was neglected. The friction force density is $q_{fric} = N\sqrt{\bar{N}}\zeta P_e D/R_e^4$. In the steady-state, it is balanced by a force density given by the functional derivative $\delta F/\delta u$:

$$\frac{\delta F}{\delta u} = q_{fric} = \frac{\partial^2}{\partial x^2}\frac{\partial f}{\partial u''}$$
$$\implies K\frac{\partial^4 u}{\partial x^4} = N\sqrt{\bar{N}}\zeta\frac{P_e D}{R_e^4}\,. \tag{5.4}$$

With the boundary conditions $u(0) = u(L) = 0$ and $u''(0) = u''(L) = 0$, one obtains:

$$u(x) = \frac{N\sqrt{\bar{N}}\zeta P_e D x}{24KR_e^4}(L^3 - 2L^2x + x^3)\,, \tag{5.5}$$

in analogy to a beam bending under a uniform load in the Euler-Bernoulli theory. The resulting lamella profile for $P_e = 0.24$ is shown in Figure 5.2. The fit is in excellent agreement with the simulation data.

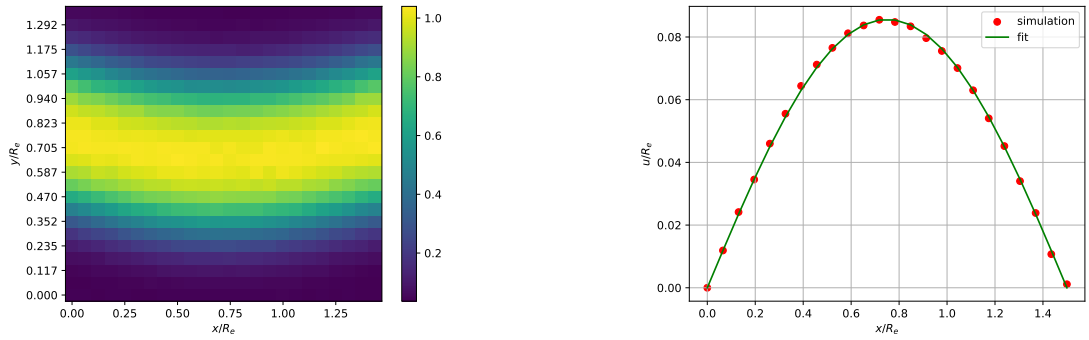

(a) (b)

Figure 5.2.: (a) Heatmap of the steady-state lamella profile in the reference frame that moves with the external field, averaged over all lamellae. (b) Lamella center of mass curve for $P_e = 0.34$. The fit corresponds to (5.5).

The maximum deformation is:

$$u_{max} = u(L/2) = \frac{5N\sqrt{\bar{N}}\zeta P_e D L^4}{384KR_e^4}\,. \tag{5.6}$$

To obtain the bending modulus, u_{max} is measured for various values of P_e, this is shown in Figure 5.3.

From (5.6), one obtains $K = 19.98\,k_BT/R_e$. Alternatively, K may also be obtained from exact SCFT. For this, the free energy of bending is computed for a

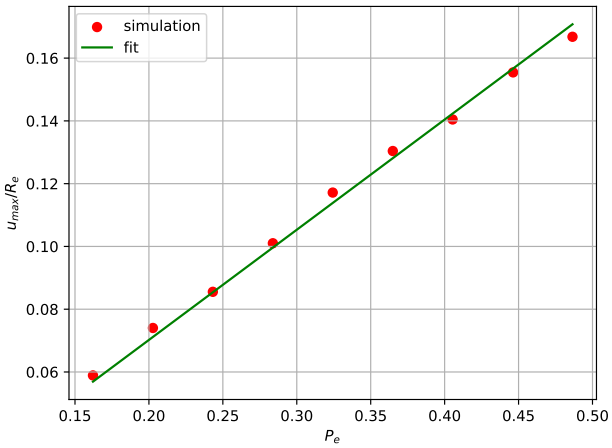

Figure 5.3.: Maximum deflection u_{max} as a function of the Péclet number P_e. The fit corresponds to (5.6).

sinusoidal deformation $u(x) = a \sin 2\pi x/L$, as shown in Figure 5.4. From (5.3), the total free energy may be calculated as:

$$\begin{aligned} F &= dL_z \int dx \left\{ f_0 + \frac{1}{2} K a^2 \left(\frac{2\pi}{L}\right)^4 \sin\left(\frac{2\pi}{L} x\right)^2 \right\} \\ &\approx dLL_z f_0 + dL_z \frac{4\pi^4 a^2}{L^3} K \,. \end{aligned} \tag{5.7}$$

On the other hand, the total free energy may be obtained by integrating over the free energy density:

$$\begin{aligned} F &= \int d\mathbf{r}(f_0 + f_b) \\ &\approx dLL_z(f_0 + f_b) \\ &= dLL_z \frac{\sqrt{\bar{N}}}{R_e^3}(\tilde{f}_0 + \tilde{f}_b) \,, \end{aligned} \tag{5.8}$$

where $\tilde{f}_0 = 4.0337\, k_B T$ is the free energy per chain of the undeformed lamella and $\tilde{f}_b = 0.79278\, k_B T (a/R_e)^2$ is the free energy per chain due to the deformation. Comparing (5.7) and (5.8), the bending modulus reads:

$$K_{\mathrm{SCFT}} = \frac{\tilde{f}_b \sqrt{\bar{N}}}{4a^2\pi^4} R_e^{-3} L^4 \,. \tag{5.9}$$

The result is $K_{\mathrm{SCFT}} = 17.47\, k_B T / R_e$, which is slightly smaller than the simulation result.

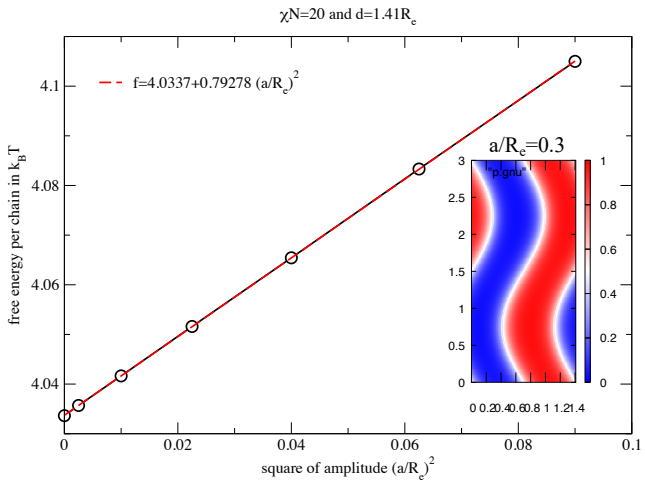

Figure 5.4.: Free energy per chain as a function of the square of the amplitude from exact SCFT calculations. The inset shows the lamella cross-section for $a/R_e = 0.3$.

6. Polymer-type-conversion-based target density

6.1. Formulation of the problem

We now want to take a step towards simulating the setting depicted in Figure 1.1. For this, we define the composition of bead-type α in cell c as:

$$\tilde{\phi}_\alpha(c) = \frac{\hat{\phi}_\alpha(c)}{\sum_{i=1}^{n_t} \hat{\phi}_i(c)} = \frac{n_\alpha(c)}{\sum_{i=1}^{n_t} n_i(c)}\,, \tag{6.1}$$

where $n_i(c)$ is the number of beads of type i in cell c. To dictate the composition in specific cells, target values $\tilde{\phi}_{\alpha,T}(c)$ are defined, with $\tilde{\phi}_{\alpha,T}(c) < 0\ \forall\alpha$ for cells in which no target composition is desired. In the following, the cells c for which $\tilde{\phi}_{\alpha,T}(c) \geq 0\ \forall\alpha$ are called "target cells". Mixed cells with $\tilde{\phi}_{\alpha,T}(c) \geq 0$ for some α and $\tilde{\phi}_{\alpha,T}(c) < 0$ for other α are not allowed and target cells must fulfill the condition $\sum_\alpha \tilde{\phi}_{\alpha,T}(c) = 1$. (**Write a test to ensure this is true!**). The total number of target cells is denoted n_T. Instead of using external fields, like in the previous section, the goal is to reach the target density by converting macromolecule types, see chapter 4. For now, only conversions between macromolecules with the same bond topology are considered. Due to the chain connectivity, this leads to a complex optimization problem for the polymer type configurations, which aims to minimize the following loss function:

$$L[\{\tilde{\phi}_i\}] = \frac{1}{n_t n_T} \sum_{\alpha=0}^{n_t} \sum_{c\in\{\text{cells}\}} \theta(\tilde{\phi}_{\alpha,T}(c)) \left(\tilde{\phi}_\alpha(c) - \tilde{\phi}_{\alpha,T}(c)\right)^2\,, \tag{6.2}$$

where $\theta(\tilde{\phi}_{\alpha,T}(c)) = 1$ if $\tilde{\phi}_{\alpha,T}(c) \geq 0$ and $\theta(\tilde{\phi}_{\alpha,T}(c)) = 0$ otherwise. Let n_f be the number of polymers that have at least one monomer in a target cell c. In the following, these polymers are called "flippable polymers". To minimise (6.2), one

must first define the notion of a neighbouring solution. If $\{\beta_1, \ldots, \beta_j, \ldots \beta_{n_f}\}$ is the current configuration of polymer types, then we define a neighbouring solution as $\{\beta_1, \ldots, \beta_j^*, \ldots \beta_{n_f}\}$, where the type of the jth polymer has been changed from β_j to β_j^* and every other polymer type is unchanged. In the following, this rule to generate a neighbouring solution is called a "flip". The flippable polymers are identified and saved to a list by algorithm 1. n_f is not constant and must be determined during runtime. The target cells in which a flippable polymer j has monomers are saved to an $n_f \times N$ matrix q_{jk}. The number of target cells $n_{cells,j}$, over which a flippable polymer j extends, varies, and is bounded by N, this is incorporated by setting $q_{jk} < 0$ for $k \geq n_{cells,j}$. Let $n_{j\beta\alpha k}$ be the $n_f \times m_t \times n_t \times N$ matrix that holds the number of monomers of type α that flippable polymer j has in target cell q_{jk} if it has the molecule type β, where $n_{j\beta\alpha k} = 0$ for $k \geq n_{cells,j}$. After the flip $\beta_j \to \beta_j^*$ of an arbitrary, flippable polymer j, the value of the loss function is updated according to:

$$\begin{aligned} L^*_{\beta_j \to \beta_j^*}[\{\tilde{\phi}_i\}] &= L[\{\tilde{\phi}_i\}] - \frac{1}{n_t n_T} \sum_{\alpha=0}^{n_t} \sum_{k=0}^{n_{cells,j}-1} \left(\tilde{\phi}_\alpha(q_{jk}) - \tilde{\phi}_{\alpha,T}(q_{jk})\right)^2 \\ &\quad + \frac{1}{n_t n_T} \sum_{\alpha=0}^{n_t} \sum_{k=0}^{n_{cells,j}-1} \left(\tilde{\phi}_\alpha(q_{jk}) + \Delta\tilde{\phi}_{j\alpha k}(\beta \to \beta^*) - \tilde{\phi}_{\alpha,T}(q_{jk})\right)^2 \\ &= L[\{\tilde{\phi}_i\}] + \frac{1}{n_t n_T} \sum_{\alpha=0}^{n_t} \sum_{k=0}^{n_{cells,j}-1} \Big\{ \Delta\tilde{\phi}^2_{j\alpha k}(\beta \to \beta^*) \\ &\quad + 2\Delta\tilde{\phi}_{j\alpha k}(\beta \to \beta^*) \left(\tilde{\phi}_\alpha(q_{jk}) - \tilde{\phi}_{\alpha,T}(q_{jk})\right) \Big\} \end{aligned} \tag{6.3}$$

where $\Delta\tilde{\phi}_{j\alpha k}(\beta \to \beta^*) \equiv \frac{n_{j\beta_j^*\alpha k} - n_{j\beta_j\alpha k}}{\sum_{i=1}^{n_t} n_i(c)}$ is the change in the composition of type α in cell q_{jk} due to the flip $\beta_j \to \beta_j^*$. Thus, for an efficient implementation of an optimization algorithm, the matrices q_{jk} and $n_{j\beta\alpha k}$ have to be determined first. How this is done with the memory structure used in SOMA is explained in algorithms 2 and 3.

6.2. Hill-climbing algorithm

In the simplest approach, flippable polymers are selected at random and flipped to a random target type. The flip is only accepted if it decreases the loss function.

n_{acc} counts the number of accepted flips. Every n_f flips, the acceptance rate $r = n_{acc}/n_f$ is calculated and n_{acc} is reset to zero until the convergence criterion $r = 0$ is fulfilled. Then, each flippable polymer is tried to be flipped one more time. Since this algorithm is only guaranteed to find a local minimum, more sophisticated optimization alogrithms may need to be employed.

6.3. Simulated annealing

If neighbouring solutions are generated by the flip of a single polymer type, (6.2) is not a convex function of the polymer type configurations, this is discussed in Figure B.1 in the appendix. Therefore, a simple hill-climbing algorithm, as discussed in the previous section, might fail at finding the global minimum. To tackle these kind of combinatorial optimization problems, the probabilistic Simulated Annealing (SA) technique [1] is frequently used. In this heuristic algorithm, a parameter T is introduced in analogy to temperature in statistical mechanics. Starting from a predefined temperature T_0, an initial guess S for the solution and a loss function L, a neighbouring solution S^* is generated by a specific rule and accepted with a probability given by the Metropolis-Hastings criterion [15]:

$$p(S \to S^*) = \min\left\{1\,, \exp\left(-\frac{L(S^*) - L(S)}{T}\right)\right\}\,. \tag{6.4}$$

Subsequently, the temperature is decreased by a predefined scheme and the procedure is repeated until a final temperature T_f is reached. A slightly modified algorithm that generates multiple neighbouring solutions for each temperature T is used in this thesis and explained in algorithm 4 in the appendix. After the annealing schedule, a few more flips are carried out at $T = 0$ using the hill-climbing algorithm until the acceptance rate reaches zero.

6.4. Comparison of algorithms

In the following, the hill-climbing algorithm is called “algorithm 1”, the SA algorithm is called “algorithm 2”. In order to compare the performance of the two algorithms, optimizations are carried out with both algorithms on several randomly generated initial configurations with different target densities. A binary system of

homopolymers with $N = 32$ and dimensions $L_x \times L_y \times L_z = 5 \times 1 \times 5\, R_e^3$ is used with $\Delta x = \Delta z = 1/8\, R_e$ and $\Delta y = 1\, R_e$ and hard walls. The number of beads per cell is varied and for each value, 100 random initial configurations are optimized and the average optimum for both algorithms is computed. $\langle L_{opt,i} \rangle$, with $i = 1, 2$, denotes the average optimum of L for algorithm i. The cooling schedule needs to be chosen in such a fashion that the acceptance rate is close to one for $T = T_0$ and approaches zero as $T \to T_f$. Specifically, the acceptance rate at a given temperature T depends on the number of beads per cell $\rho_{cell} = nN/n_{cells}$. An exponential cooling schedule is applied:

$$T_k = T_0 \alpha^k \,, \tag{6.5}$$

with $T_0 = 1.0$, $\alpha = 0.85$ and $k_{max} = 57$, which corresponds to $T_f = 10^{-4}$. This schedule was found to be appropriate for the considered range of $\rho_{cell} = 0.2 \ldots 10.0$, see Figure 6.1.

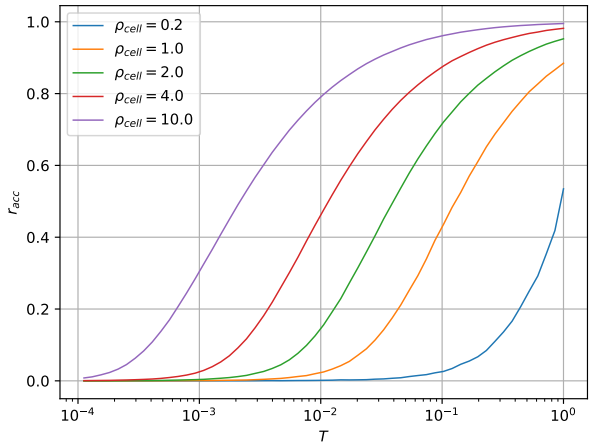

Figure 6.1.: Acceptance rate for different values of ρ_{cell}.

The optimum values are rescaled by the density variance predicted by the mean field approximation $\sigma_0^2 = \rho_0 V_c \kappa$ [5].

Algorithm 2 is slower and does not significantly improve the optimum, especially for large values $\sqrt{N}$.

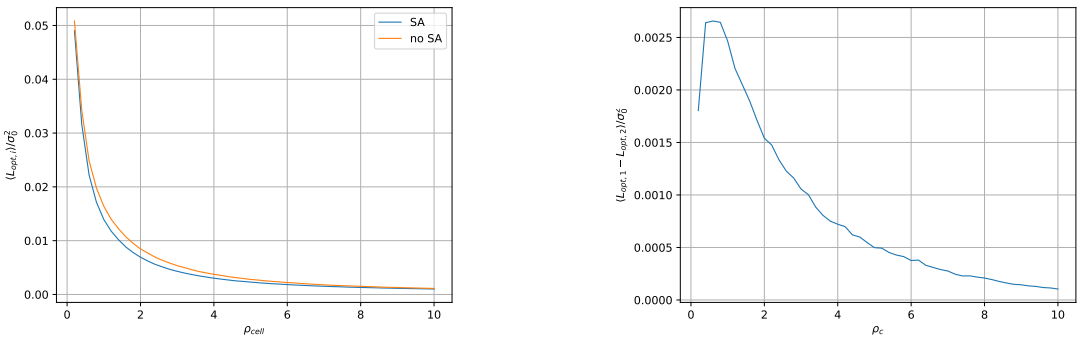

(a) (b)

Figure 6.2.: $\Delta\tilde{\phi} = 0$ (a) Mean squared deviation from target density for $\Delta L = 1/8\, R_e$ and different values of $\sqrt{\bar{N}}$. (b) Difference

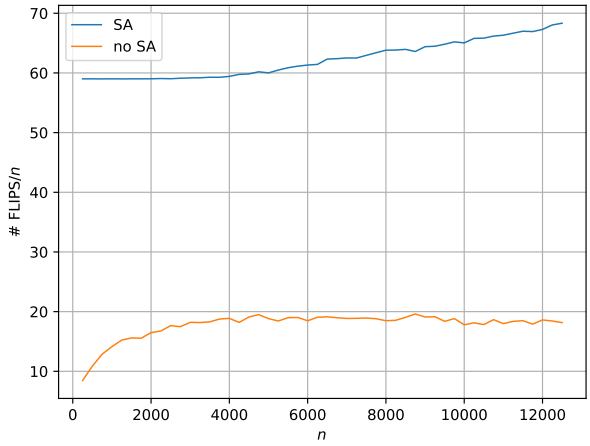

Figure 6.3.: Number of flips until convergence for both algorithms.

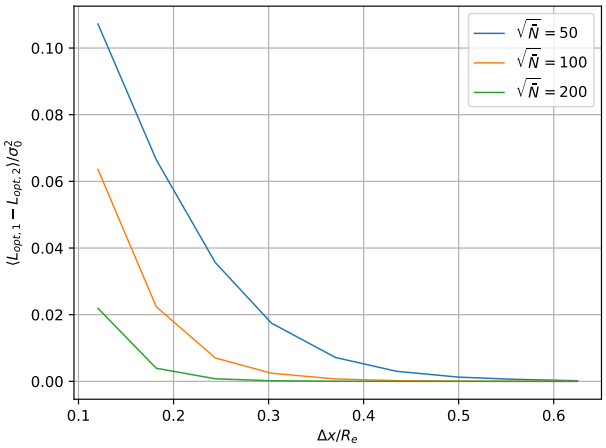

Figure 6.4.: Difference for different discretizations.

7. Outlook

- Still the old version from Einfuehrung ins Wissenschaftliche Arbeiten

The collective diffusion coefficient of a symmetric homopolymer mixture under a boundary-driven diffusion flux has been studied. In the future, more sophisticated and time-dependent boundary conditions will be employed to manipulate the behavior of the bulk, with the ultimate goal of simulating smaller sections of a large continuum simulation using particle-based simulations. The key question is whether or not the time evolution of the boundary densities is sufficient to dictate the time-evolution of the densities in the bulk. An approach based purely on center-of-mass-based polymer conversion zones might be problematic due to the extension of the converted chains beyond the boundaries. Simple conversions without changing the position of the beads may also lead to unlikely configurations of the affected polymer, so it might be necessary to let the chain grow into the simulation box, e.g. using the configurational bias method [27].

A. Algorithms

Algorithm 1 Get flippable polymers

```
Let polyIsflippable[n] be a new boolean array initialised with 0's
n_f ← 0
for poly ← 0 to n − 1 do
    for monomer ← 0 to N − 1 do
        monoCell ← poly.beads[monomer].cell
        if Target density available for monoCell then
            polyIsflippable[poly] ← 1
            n_f ← n_f + 1
            break
        end if
    end for
end for
Let polyFlippableIndices[n_f] be a new array
i ← 0
for poly ← 0 to n − 1 do        ▷ Store indices of flippable polymers to new array
    if polyIsflippable[poly] == 1 then
        polyFlippableIndices[j] ← poly
        j ← j + 1
    end if
end for
```

Algorithm 2 Get cell index matrix

```
Let polyCellIndices[n_f][N] be a new array initialised with −1's
for i ← 0 to n_f − 1 do                                  ▷ Loop over flippable polymers
    poly ← polymers[polyFlippableIndices[i]]
    let monoCells[N] be a new array
    j ← 0
    for monomer ← 0 to N − 1 do
        if Target density available for monoCell then
            monoCells[j] ← poly.beads[monomer].cell
            j ← j + 1
            break
        end if
    end for
    quicksort(monoCells , 0 , j − 1)
    k ← 0
    for monomer ← 0 to j − 1 do                                  ▷ Find unique cells
        if monoCells[monomer] ≠ monoCells[monomer + 1] then
            polyCellIndices[i][k] ← monoCells[monomer]
            k ← k + 1
        end if
    end for
    polyCellIndices[i][k] ← monoCells[j − 1]
end for
```

Algorithm 3 Get cell number matrix

Let $polyCellNum[n_f][m_t][n_t][N]$ be a new array initialised with 0's
for $i \leftarrow 0$ to $n_f - 1$ **do** ▷ Loop over flippable polymers
  $poly \leftarrow polymers[polyFlippableIndices[i]]$
  $initialPolytype \leftarrow poly.type$
  for $polyType \leftarrow 0$ to $n_t - 1$ **do**
    $poly.type \leftarrow polyType$ ▷ Temporarily change polymer type
    for $monomer \leftarrow 0$ to $N - 1$ **do**
      $monoCell \leftarrow poly.beads[monomer].cell$
      $monoType \leftarrow poly.beads[monomer].type$
      for $j \leftarrow 0$ to $N - 1$ **do** ▷ Find corresponding entry
        if $polyCellIndices[i][j] == monoCell$ **then**
          $polyCellNum[i][polyType][monoType][j]++$
          break
        end if
      end for
    end for
  end for
  $poly.type \leftarrow initialPolytype$ ▷ Restore polymer type
end for

Algorithm 4 Simulated annealing

$S \leftarrow$ current configuration of polymer types
$T \leftarrow T_0$
while $T > T_f$ **do**
  $n_{flip} \leftarrow 0$
  while $n_{flip} < n_{max}$ **do**
    Generate new configuration S^* by flipping a random polymer
    $n_{flip} \leftarrow n_{flip} + 1$
    $\Delta L \leftarrow L(S^*) - L(S)$
    $r \leftarrow$ random number between 0 and 1
    if $r < \exp(-\frac{\Delta L}{T})$ **then**
      $S \leftarrow S^*$
    end if
  end while
  $T \leftarrow \alpha * T$ ▷ or different cooling schedule
end while

B. Optimization problem

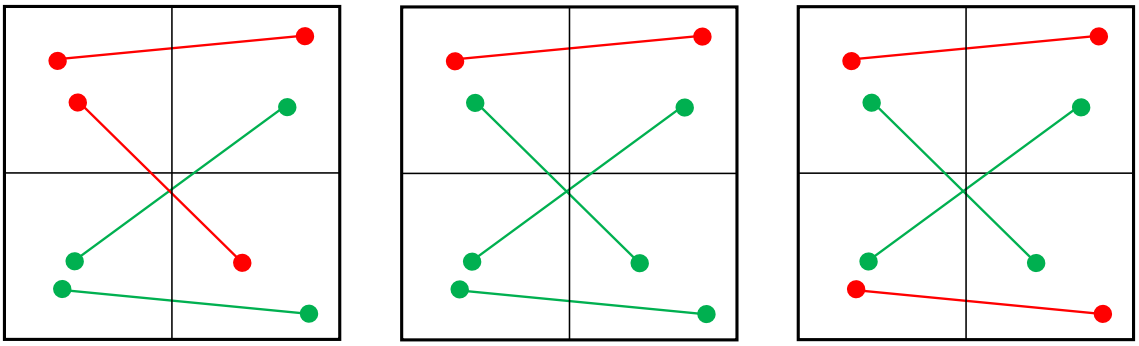

(a) (b) (c)

Figure B.1.: Example for $n = 4$ homopolymers with $N = 2$ on a 2×2 grid to show that the loss function defined by (6.2) is in general non-convex in the polymer type configurations, where a neighbouring solution is defined as a configuration of polymer types, where only a single polymer type is changed. Different colours denote different types. The target compositions are $\tilde{\phi}_{\mathrm{A},T} = \tilde{\phi}_{\mathrm{B},T} = 0.5$ for all cells. In (a), any possible flip will not lead to a better value of L. (b) shows the configuration after conversion of a red polymer to a green one. A flip of the lower polymer now leads to a decrease of the loss function, as shown in (c). Note that this minimum is not unique, since a flip of every polymer would also yield $L = 0$.

Bibliography

[1] Optimization by simulated annealing. *Science*, 220(4598):671–680, 1983. doi: 10.1126/science.220.4598.671. URL https://www.science.org/doi/abs/10.1126/science.220.4598.671.

[2] J. Baschnagel, H. Meyer, F. Varnik, S. Metzger, M. Aichele, M. Müller, and K. Binder. Computer simulations of polymers close to solid interfaces: Some selected topics. *Interface Science*, 11(2):159–173, 2003. doi: 10.1023/A:1022118610890. URL https://doi.org/10.1023/A:1022118610890.

[3] Frank S. Bates, Wayne W. Maurer, Paul M. Lipic, Marc A. Hillmyer, Kristoffer Almdal, Kell Mortensen, Glenn H. Fredrickson, and Timothy P. Lodge. Polymeric bicontinuous microemulsions. *Phys. Rev. Lett.*, 79:849–852, Aug 1997. doi: 10.1103/PhysRevLett.79.849. URL https://link.aps.org/doi/10.1103/PhysRevLett.79.849.

[4] K. Binder. Collective diffusion, nucleation, and spinodal decomposition in polymer mixtures. *The Journal of Chemical Physics*, 79(12):6387–6409, 1983. doi: 10.1063/1.445747. URL https://doi.org/10.1063/1.445747.

[5] Kostas Ch. Daoulas and Marcus Müller. Single chain in mean field simulations: Quasi-instantaneous field approximation and quantitative comparison with monte carlo simulations. *The Journal of Chemical Physics*, 125(18):184904, 2006. doi: 10.1063/1.2364506. URL https://doi.org/10.1063/1.2364506.

[6] P. G. de Gennes. Dynamics of fluctuations and spinodal decomposition in polymer blends. *The Journal of Chemical Physics*, 72(9):4756–4763, 1980. doi: 10.1063/1.439809. URL https://doi.org/10.1063/1.439809.

[7] Oliver Dreyer, Gregor Ibbeken, Ludwig Schneider, Niklas Blagojevic, Maryam Radjabian, Volker Abetz, and Marcus Müller. Simulation of solvent evaporation from a diblock copolymer film: Orientation of the cylindrical mesophase.

Macromolecules, 55(17):7564–7582, 2022. doi: 10.1021/acs.macromol.2c00612. URL https://doi.org/10.1021/acs.macromol.2c00612.

[8] Dominik Düchs, Venkat Ganesan, Glenn H. Fredrickson, and Friederike Schmid. Fluctuation effects in ternary ab + a + b polymeric emulsions. *Macromolecules*, 36(24):9237–9248, 12 2003. doi: 10.1021/ma030201y. URL https://doi.org/10.1021/ma030201y.

[9] A. Einstein. Über die von der molekularkinetischen theorie der wärme geforderte bewegung von in ruhenden flüssigkeiten suspendierten teilchen. *Annalen der Physik*, 322(8):549–560, 1905. doi: https://doi.org/10.1002/andp.19053220806. URL https://onlinelibrary.wiley.com/doi/abs/10.1002/andp.19053220806.

[10] I Ya Erukhimovich and AN Semenov. Nonexponential density relaxation and the dynamic form-factor of polymer melts in the reptation regime. *Zh. Eksp. Teor. Fiz*, 63:275, 1986.

[11] Paul J. Flory. Thermodynamics of high polymer solutions. *The Journal of Chemical Physics*, 10(1):51–61, 1942. doi: 10.1063/1.1723621. URL https://doi.org/10.1063/1.1723621.

[12] J. G. E. M. Fraaije, B. A. C. van Vlimmeren, N. M. Maurits, M. Postma, O. A. Evers, C. Hoffmann, P. Altevogt, and G. Goldbeck-Wood. The dynamic mean-field density functional method and its application to the mesoscopic dynamics of quenched block copolymer melts. *The Journal of Chemical Physics*, 106(10):4260–4269, 1997. doi: 10.1063/1.473129. URL https://doi.org/10.1063/1.473129.

[13] Ludwik Leibler. Theory of microphase separation in block copolymers. *Macromolecules*, 13(6):1602–1617, 1980.

[14] R.H. Colby M. Rubinstein. *Polymer Physics*. Oxford University Press, 2003.

[15] Nicholas Metropolis, Arianna W. Rosenbluth, Marshall N. Rosenbluth, Augusta H. Teller, and Edward Teller. Equation of State Calculations by Fast Computing Machines. *The Journal of Chemical Physics*, 21(6):1087–1092, 12 2004. ISSN 0021-9606. doi: 10.1063/1.1699114. URL https://doi.org/10.1063/1.1699114.

[16] M. Müller and G. Gompper. Elastic properties of polymer interfaces: Aggregation of pure diblock, mixed diblock, and triblock copolymers. *Phys. Rev. E*, 66:041805, Oct 2002. doi: 10.1103/PhysRevE.66.041805. URL `https://link.aps.org/doi/10.1103/PhysRevE.66.041805`.

[17] Marcus Müller. Studying amphiphilic self-assembly with soft coarse-grained models. *Journal of Statistical Physics*, 145:967–1016, 11 2011. doi: 10.1007/s10955-011-0302-z.

[18] Marcus MÃ¼ller and Kostas Ch. Daoulas. Single-chain dynamics in a homogeneous melt and a lamellar microphase: A comparison between Smart Monte Carlo dynamics, slithering-snake dynamics, and slip-link dynamics. *The Journal of Chemical Physics*, 129(16), 10 2008. ISSN 0021-9606. doi: 10.1063/1.2997345. URL `https://doi.org/10.1063/1.2997345`. 164906.

[19] C. Pangali, M. Rao, and B.J. Berne. On a novel monte carlo scheme for simulating water and aqueous solutions. *Chemical Physics Letters*, 55(3): 413–417, 1978. ISSN 0009-2614. doi: https://doi.org/10.1016/0009-2614(78)84003-2. URL `https://www.sciencedirect.com/science/article/pii/0009261478840032`.

[20] C. Pangali, M. Rao, and B.J. Berne. On a novel monte carlo scheme for simulating water and aqueous solutions. *Chemical Physics Letters*, 55(3): 413–417, 1978. ISSN 0009-2614. doi: https://doi.org/10.1016/0009-2614(78)84003-2. URL `https://www.sciencedirect.com/science/article/pii/0009261478840032`.

[21] Shuanhu Qi and Friederike Schmid. Hybrid particle-continuum simulations coupling brownian dynamics and local dynamic density functional theory. *Soft Matter*, 13:7938–7947, 2017. doi: 10.1039/C7SM01749A. URL `http://dx.doi.org/10.1039/C7SM01749A`.

[22] Ellen Reister. *Zusammenhang zwischen der Einzelkettendynamik und der Dynamik von Konzentrationsfluktuationen in mehrkomponentigen Polymersystemen*. PhD thesis, Mainz, 2002.

[23] Peter J. Rossky, Jimmie D. Doll, and Harold L. Friedman. Brownian dynamics as smart monte carlo simulation. *Journal of Chemical Physics*, 69:4628–4633, 1978.

[24] Prince E. Rouse. A theory of the linear viscoelastic properties of dilute solutions of coiling polymers. *The Journal of Chemical Physics*, 21(7):1272–1280, 1953. doi: 10.1063/1.1699180. URL `https://doi.org/10.1063/1.1699180`.

[25] Ludwig Schneider and Marcus Müller. Multi-Architecture Monte-Carlo (MC) Simulation of Soft Coarse-Grained Polymeric Materials: SOft coarse grained Monte-carlo Acceleration (SOMA). *arXiv e-prints*, art. arXiv:1711.03828, November 2017. doi: 10.48550/arXiv.1711.03828.

[26] A. N. Semenov. Theory of Long-Range Interactions in Polymer Systems. *J. Phys. II*, 6(12):1759–1780, December 1996. ISSN 1155-4312. doi: 10.1051/jp2:1996159.

[27] Jörn Ilja Siepmann and Daan Frenkel. Configurational bias monte carlo: a new sampling scheme for flexible chains. *Molecular Physics*, 75(1):59–70, 1992. doi: 10.1080/00268979200100061. URL `https://doi.org/10.1080/00268979200100061`.

[28] Glenn M. Torrie and John P. Valleau. Monte carlo free energy estimates using non-boltzmann sampling: Application to the sub-critical lennard-jones fluid. *Chemical Physics Letters*, 28(4):578–581, 1974. ISSN 0009-2614. doi: https://doi.org/10.1016/0009-2614(74)80109-0. URL `https://www.sciencedirect.com/science/article/pii/0009261474801090`.

[29] Zhen-Gang Wang. Response and instabilities of the lamellar phase of diblock copolymers under uniaxial stress. *The Journal of Chemical Physics*, 100(3):2298–2309, 02 1994. ISSN 0021-9606. doi: 10.1063/1.466528. URL `https://doi.org/10.1063/1.466528`.